Spatially resolved simulation of coronary hemodynamics

M. Neumann, F. Neumann, R. Karch, W. Schreiner

Institute of Experimental Physics, Dept. of Surgery & Dept. of Medical Computer Sciences, University of Vienna, A-1090 Wien, Austria

Abstract

Computer-generated "realistic" structures of arterial trees consisting of 8000 segments have been used as a basis for computer simulations of coronary hemodynamics. For the perfusion pressure, a synthesized wave form typical of the aortic pressure was used, while the temporally varying intramyocardial pressure was related to the (also) synthesized left ventricular pressure. The elastic properties of the vessel segments were derived from a simple *ad-hoc* model of arterial compliance. The model yields the typical wave form of pulsatile coronary flow. The variability of coronary flow patterns resulting from variations in the way intramyocardial squeezing is applied has been investigated in detail.

1 Introduction

The wave form of coronary artery blood flow is characterized by the interplay between two mechanisms: the driving pressure of the aorta inducing a pressure gradient along the whole coronary vascular system, and the squeezing pressure of the myocardium, which limits blood flow during systolic contraction by increasing the resistance of the vessel tree. Computer simulation of coronary hemodynamics has to take into account this particular pressure dynamics as well as the structure of the system and the compliance of its constituent vessels.

In the past, simulation studies of coronary hemodynamics mostly used either compartmental models, multi-layer models, or stochastic network models. Even in the latter—although vessel segments are considered in detail—their geometrical arrangement is not necessarily realistic. In con-

40   Simulation Modelling in Bioengineering

trast, the present simulations are based on computer-generated "realistic" structures of arterial trees generated by "constrained constructive optimization" (CCO). These model trees consist of $O(10^4)$ cylindrical segments which provide a uniform blood supply to a (presently two-dimensional) perfusion area (Schreiner[1]).

In such a model tree spatial and temporal distribution of pressures and flow can, for the first time, be analyzed in detail from the root segment ($r \approx 1.5\,\mathrm{mm}$) down to small segments with radii of approximately $50\,\mu$. In the hemodynamic simulations, the arterial tree is represented by a network of non-linear elements. This is numerically equivalent to solving the one-dimensional hydrodynamic equations. For the compliance of individual vessel segments, a simple *ad-hoc* model has been developed, which was based on an experimentally established relationship between vessel radius and wall thickness (Podesser *et al.*[2]). Without further assumptions, this model yields the characteristic wave forms of pulsatile coronary artery flow. Redistribution of flow resulting from changes in the geometrical and functional properties of the tree, in the elastic properties of the segments, or from variations in the way intramyocardial squeezing is applied, may be investigated in arbitrary detail.

2 CCO trees of coronary arteries

In our method of constrained constructive optimization, an arterial tree is created in full detail from the feeding artery down to individual terminal segments. Based on realistic considerations of blood supply and nutrition of myocardial tissue, the model trees are grown according to given boundary conditions, a set of constraints, and an optimization target (Schreiner *et al.*[3]). Resistance and flow conditions in the trees are assumed to obey Poiseuille's law. Table 1 shows the model parameters for pressures and flows chosen to perfuse a (two-dimensional) piece of tissue which roughly corresponds to the myocardial region fed by the left coronary artery in humans. Usually a circle of $5\,\mathrm{cm}$ radius is used as perfusion area supporting the simulated tree structure. Due to the rigorously dichotomous branching pattern, the total number of segments is determined by the number of terminal segments as $N_{\mathrm{tot}} = 2N_{\mathrm{term}} - 1$, regardless of the particular structure of a tree.

The radii of parent and daughter segments at each bifurcation are assumed to obey a power law

$$r_{\mathrm{parent}}^{\gamma} = r_{\mathrm{left}}^{\gamma} + r_{\mathrm{right}}^{\gamma}. \tag{1}$$

In the model tree shown in Fig. 1, the exponent was set to $\gamma = 3$, which is compatible with uniform shear stress throughout the whole tree (Rodbard[4]).

Table 1: Global model parameters

parameter		preset value
A_{perf}	size of perfusion area	78.54 cm^2
p_{perf}	perfusion pressure	100 mm Hg
p_{term}	terminal pressure	60 mm Hg
Q_{perf}	perfusion flow	500 ml/min
N_{term}	number of terminals	4000
Q_{term}	terminal flow	$Q_{\text{perf}} / N_{\text{term}}$

The model tree is grown by successive addition of terminal segments and generation of new bifurcations. At each step, segment radii are rescaled in order to maintain the global constraints and to obey the bifurcation law of Eq. (1). Since this can be achieved for arbitrary locations of a new bifurcation within the existing tree, it is necessary to introduce a criterion for the "optimum" placement of that bifurcation. Optimality may be defined in terms of the functional structure, and global properties of the tree, such as total surface or volume, are suitable cost functions. The cost (or target) function chosen here is of the general type

$$T = \sum_{i=1}^{N_{\text{tot}}} \ell_i \, r_i^\lambda \to \min, \qquad (2)$$

where ℓ_i and r_i are length and radius of segment i. In the CCO tree of Fig. 1, the exponent λ was set to 2, which, apart from a multiplicative factor, is equivalent to minimizing total intravasal volume of the tree. Minimizing the target function not only optimizes the geometrical location of a single bifurcation on a given segment, but also governs the development of the global topological structure of the tree (see Schreiner et al.[5]).

3 Model of arterial compliance

Constrained constructive optimization of arterial trees provides the connective structure and positions, as well as the inner radii and vessel lengths of individual segments. In the optimization process, all segments are considered to be rigid cylindrical tubes. However, in order to investigate the hemodynamic properties of arterial trees under "realistic" conditions of aortic pressure and intramyocardial squeezing, it is also necessary to specify a compliance for each segment, which is essentially determined by the thickness of the vessel wall and its elastic properties. In CCO trees, where the radii of vessel segments span a range from 50 to 1500 μ, the large proximal segments may be expected to have rather thin, but highly compliant walls, whereas distal vessels will be narrow, thick-walled, and increasingly stiff.

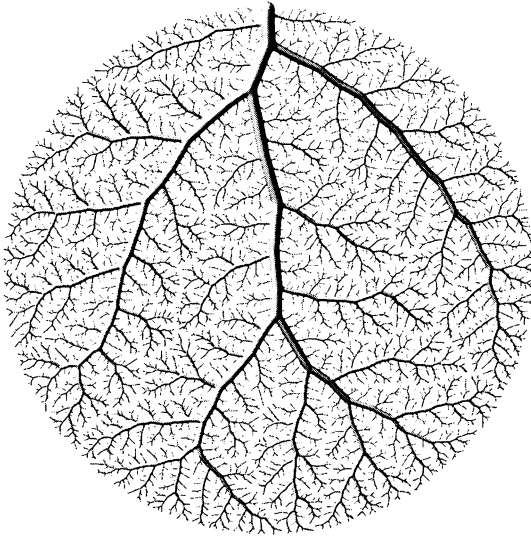## 42   Simulation Modelling in Bioengineering

Figure 1: CCO-generated arterial model tree used as a basis for computer simulation of the coronary hemodynamics.

As could be shown by experimental measurements within our group, the relation between wall thickness h and vessel radius r for human coronary arteries can be approximately represented by a power law (Fig. 2, Podesser *et al.*[2])

$$h = ar^b . \tag{3}$$

Fitting Eq. (3) on a logarithmic scale to the data of [2] yields $a = 2.54 \pm 0.25$ and $b = 0.476 \pm 0.044$, if h and r are measured in μ. In order to arrive at a manageable closed expression for the arterial compliance which qualitatively describes the elastic properties of vessels differing in size by almost three orders of magnitude, we have made a number of drastic simplifications: All segments are made up of the same homogeneous incompressible material. Vessel lengths are constant, and viscoelastic and hysteresis effects are neglected. Wall tension σ and stretch ratio S are assumed to be related by

$$\frac{\partial \sigma}{\partial S} = E_0 + E_1 \sigma, \tag{4}$$

which is approximately realized in actual arterial trees (Fung[6]). The parameters

$$
\begin{aligned}
E_0 &= 5000 \text{ mm Hg} \\
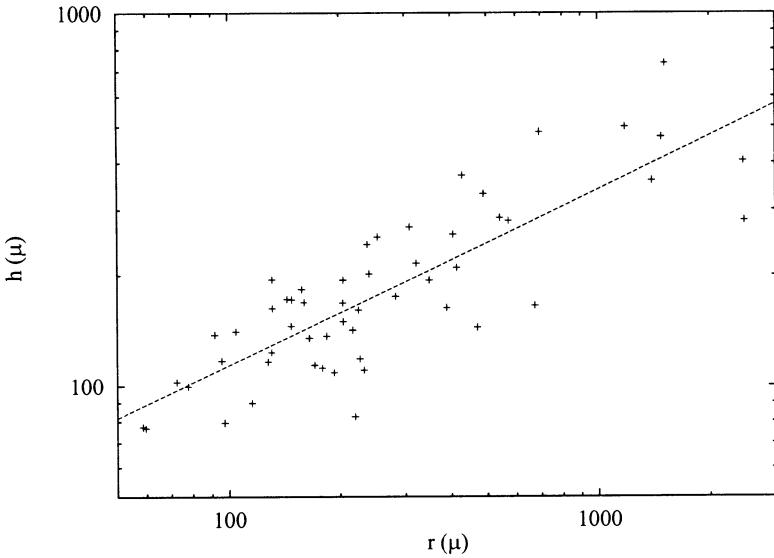\text{and} \quad E_1 &= 30
\end{aligned}
$$

Figure 2: Radius and wall thickness of human coronary arteries. A power law [dashed line, Eq. (3)] fitted to the data of Podesser *et al.* [2] is used to define a global model of arterial compliance.

were chosen so as to reproduce some of the rare literature data (Douglas *et al.*[7], Gow *et al.*[8]), in which elastic properties of (large) epicardial arteries of specified radius *and wall thickness* are reported over an extended pressure range. Furthermore, we have assumed that Laplace's law for infinitely thin-walled tubes (Fung[6])

$$\sigma = \frac{(p_{\text{int}} - p_{\text{ext}})r}{h} - p_{\text{ext}} , \qquad (5)$$

where p_{int} is the internal (intravasal) and p_{ext} the external (intramyocardial) pressure, may also be used for vessels of finite wall thickness.

Putting all this together, we obtain the following pressure-radius relationship

$$\frac{(p_{\text{int}} - p_{\text{ext}})\, r}{\sqrt{r^2 + 2r_0 h_0 + h_0{}^2} - r} - p_{\text{ext}} =$$

$$\frac{E_0}{E_1} \left\{ \exp\left[E_1 \left(\frac{r + \sqrt{r^2 + 2r_0 h_0 + h_0{}^2}}{2r_0 + h_0} - 1 \right) \right] - 1 \right\} , \qquad (6)$$

which describes how the (inner) radius r of a segment changes with internal

44   Simulation Modelling in Bioengineering

pressure p_{int} and external pressure p_{ext}. r_0 and h_0 denote radius and wall thickness in the pressure-free state $(p_{int} = p_{ext} = 0)$. Together with E_0 and E_1 these parameters completely specify the elastic behavior of an individual segment. Figure 3 illustrates this relation for an epicardial artery with a relaxed radius of $r_0 = 1.5\,\text{mm}$ and h_0 calculated by means of Eq. (3).
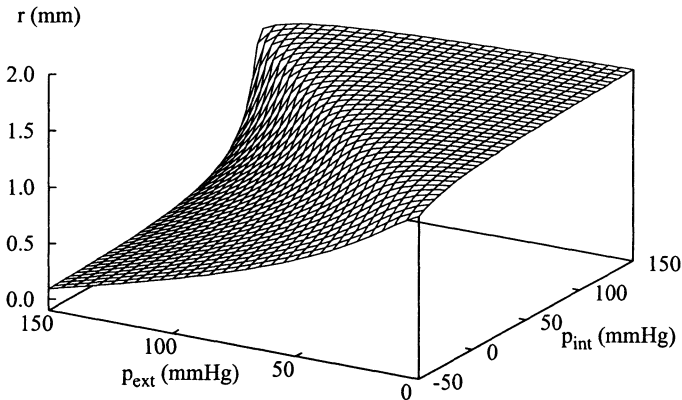

Figure 3: Dependence of the radius of a large coronary artery $(r_0 = 1.5\,\text{mm})$ on internal blood pressure p_{int} and external squeezing pressure p_{ext}.

It is apparent that this simple model of vascular compliance is capable of reproducing the qualitative properties of real arteries, such as the sigmoidal variation of the vessel radius with internal pressure p_{int}, or the vessel collapse at high intramyocardial pressure p_{ext}. It is also evident that the vessel radius depends not only on transmural pressure $p_{int} - p_{ext}$ alone, but is determined by the individual values of p_{int} and p_{ext}.

In order to validate the model, it was applied to all segments of a number of complete CCO trees, and the global properties of the trees were determined and compared to data from the literature. In particular, we investigated the specific compliance of the arterial bed and the stationary pressure-flow relationship as a function of (temporally constant) perfusion pressure. In trees with different parameters for the bifurcation law [γ, Eq. (1)] and for the target function [λ, Eq. (2)] we found good qualitative agreement between our model results and the available experimental data (Neumann et al.[9]).

4 Simulation of flow in coronary arteries

4.1 Methods

Since a numerical simulation of time-dependent flow in a system of several thousand segments based on the full three-dimensional hydrodynamic equations is not feasible in practice, even arterial trees with substantially fewer segments are often treated by means of the reduced one-dimensional Navier-Stokes equations (e.g. Rooz[10], Wiesner [11]). Under the specific conditions of pulsatile hemodynamics, these equations are numerically equivalent to the "telegraph equations" of transmission-line theory, if blood pressure and flow are interpreted as voltage and current, respectively (Milnor[12]).
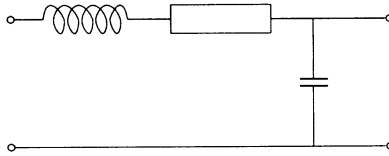
Figure 4: RLC circuit representing an individual segment of the CCO tree.

We have used this well-known analogy to replace each segment of a CCO tree by a simple non-linear electrical RLC circuit of the type shown in Fig. 4. Since most segments in our CCO trees are very short, this may be interpreted as an approximate spatial discretization of the telegraph equations for leakage-free conditions. In the framework of an electrical analog model, the equivalent of the hydrodynamical momentum equations is (cf. Rideout[13])

$$L_i \frac{dQ_i}{dt} = (p_{\text{int,p}(i)} - p_{\text{int},i}) - R_i Q_i \,, \tag{7}$$

where $p_{\text{int},i}$ is the intravasal pressure at the distal end of segment i, Q_i is the proximal flow into i, and the subscript p(i) denotes the parent segment of i. Resistance R_i and inductance L_i of segment i are given by

$$R_i = \frac{8\eta \, \ell_i}{r_i^4 \, \pi} \tag{8}$$

$$L_i = \frac{\rho \, \ell_i}{r_i^2 \, \pi} \,, \tag{9}$$

where r_i and ℓ_i are radius and length of segment i, and η and ρ are viscosity and mass density of blood. Equation (8) is based on the validity of Poiseuille's law which is, of course, a debatable assumption. Since the segment radius is determined by the pressure-radius relationship, Eq. (6), R_i

46   Simulation Modelling in Bioengineering

and L_i are both dependent on pressure, and Eq. (7) is therefore a non-linear differential equation.

For the same reason, the capacitance (or compliance), which is normally given by

$$C_i = 2 r_i \, \pi \, \ell_i \frac{\partial r_i}{\partial p_{\text{int},i}} \tag{10}$$

is also pressure-dependent. However, this relation is not immediately applicable unless p_{ext} is constant. Since, in our case, the radius depends explicitly on both p_{int} and p_{ext}, volume changes are related to pressure changes by

$$
\begin{aligned}
dV_i &= 2 r_i \, \pi \, \ell_i \left[\frac{\partial r_i}{\partial p_{\text{int},i}} dp_{\text{int},i} + \frac{\partial r_i}{\partial p_{\text{ext},i}} dp_{\text{ext},i} \right] \\
&= C_i \left[dp_{\text{int},i} + \frac{\partial r_i / \partial p_{\text{ext},i}}{\partial r_i / \partial p_{\text{int},i}} dp_{\text{ext},i} \right]
\end{aligned}
\tag{11}
$$

Therefore, the equivalent of the equation of continuity may be written as

$$C_i \left[\frac{dp_{\text{int},i}}{dt} + \frac{\partial r_i / \partial p_{\text{ext},i}}{\partial r_i / \partial p_{\text{int},i}} \frac{dp_{\text{ext},i}}{dt} \right] = Q_i - \left(Q_{\text{l}(i)} + Q_{\text{r}(i)} \right), \tag{12}$$

where $Q_{\text{l}(i)}$ and $Q_{\text{r}(i)}$ is the flow into the left and right daughter segment of i. For the calculation of $\partial r_i / \partial p_{\text{int},i}$ the arithmetic average of distal and proximal pressures is used.

Equations (7) and (12) form a system of coupled ordinary differential equations which were solved by Cromer's method (Cromer[14]). This is a simple, but stable algorithm for the integration of coupled first-order equations with oscillatory solutions. Basically, the pressure and flow equations were both integrated using a simple Euler method: the flow equations, Eq. (7), were solved by means of the explicit scheme, and the pressure equations, Eq. (12), by means of the implicit scheme using the freshly calculated flows on the right-hand side. Since, in order to calculate the coefficients in Eqs. (7) and (12), the transcendental pressure-radius relationship of Sec. 3 has to be solved for r_i at every time step, the coefficients in the pressure equations were allowed to lag behind by one time step.

4.2 Results

The characteristic shape of flow waves in the coronary arteries is the result of an interplay between two mechanisms: a driving pressure, or pressure gradient, given essentially by the difference between the aortic pressure (AoP) and the pressure level at the (microcirculatory) terminals of the arterial tree; and the variation of vascular resistance due to intramyocardial squeezing. The intramyocardial pressure (IMP), which is responsible for the periodic
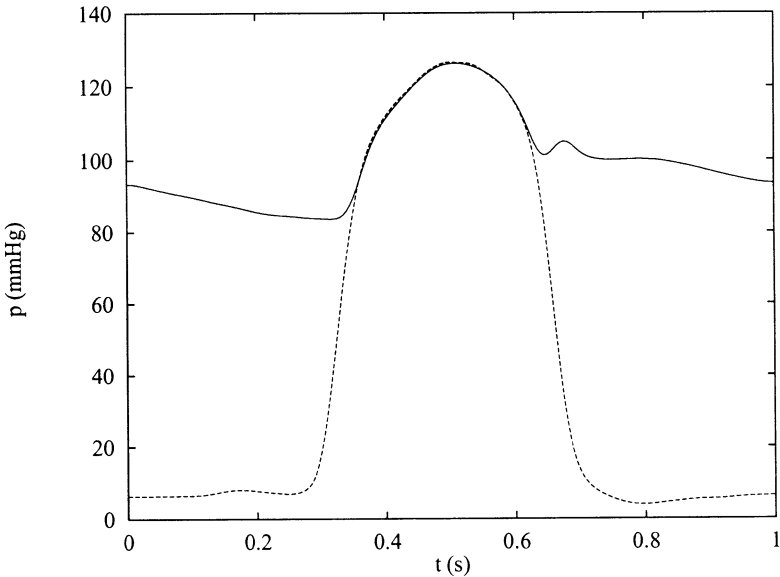
Figure 5: Fourier-synthesized typical wave forms of aortic pressure (solid line) and left ventricular pressure (dashed line) as used for the flow simulation shown in Fig. 6.

reduction of vessel dimensions, is in the present work assumed to be spatially homogeneous and proportional to left ventricular pressure (LVP). It is the temporal relation between AoP and IMP, their respective amplitudes, and the vascular compliance which determine systolic flow impediment and diastolic perfusion of the myocardium.

In our exploratory simulation studies, AoP and IMP were represented by Fourier-synthesis (cf. Fig. 5) using digitized textbook curves (Milnor[12]), while the distal pressure was kept constant at 60 mm Hg for all terminal segments. All simulations were started from the steady state conditions underlying CCO (cf. Table 1), by suddenly switching on a time varying pressure corresponding to a heart rate of 60 bpm. The pulsatile driving pressure applied to the proximal end of the root segment was taken to be AoP, or a phase-shifted version of AoP delayed by a small time lag. Optionally, all segments were also subjected to an intramyocardial squeezing pressure proportional to the Fourier-synthesized LVP. After a transient stage, a periodic solution was obtained by integrating the differential equations, Eqs. (7) and (12), for about five heart beats (cycles).

Figures 6 and 7 provide a few selected examples which demonstrate that the present approach not only yields very realistic flow-wave forms, but also allows us to study the dependence of global and spatio-temporally resolved hemodynamic observables on the features of the underlying model. This is
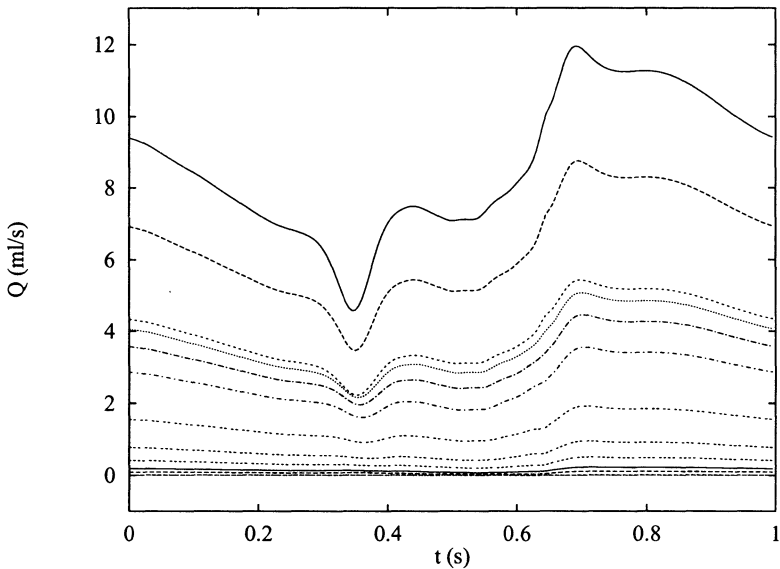
Figure 6: Resulting flow in the root (top curve) and every 10th segment along the main vessel, if the pressures given in Fig. 5 are applied to the CCO tree shown in Fig. 1. Full myocardial squeezing, i.e. IMP=LVP.

achieved with a minimum of adjustable parameters and despite the drastic approximations made in formulating a simple mathematical relationship for the vascular compliance.

Figure 6 shows the pulsatile flow in the root and every tenth segment along the main vessel of the CCO tree of Fig. 1. (The main vessel is the set of segments obtained by starting at the root and always choosing the larger daughter segment at successive bifurcations.) The curves exhibit the wave form typical of coronary flow and a progressive damping as one moves from the root towards the terminal segment.

The sensitivity of total arterial inflow to the time lag between driving pressure and intramyocardial squeezing is investigated in Fig. 7. The delay was produced by simply shifting AoP backwards in time with respect to IMP (i.e. LVP). The effect of a 20 ms (dashed) or 50 ms (dash-dotted) delay is an increasingly more pronounced minimum at the beginning of systole, compared to perfectly synchronized AoP and LVP (full line). On the other hand, leaving AoP and LVP synchronized, but increasing IMP uniformly by 10 % (i.e. IMP= $1.1 \times$ LVP) leads to a significantly reduced flow throughout the entire systolic phase (dotted line). For comparison, the wave form corresponding to completely unhindered flow, with intramyocardial squeezing switched off, is also given (circles).

These examples clearly demonstrate that rather minor changes in the pressure conditions may have a profound influence on myocardial perfusion. Such changes and their consequences may be decisive for the effectiveness and benefit of therapeutic interventions. It is therefore evident that computer simulation is not only a convenient technique for modeling and understanding coronary hemodynamics, but also an essential tool for quantitatively estimating the possible therapeutic effects of cardiological and surgical interventions.
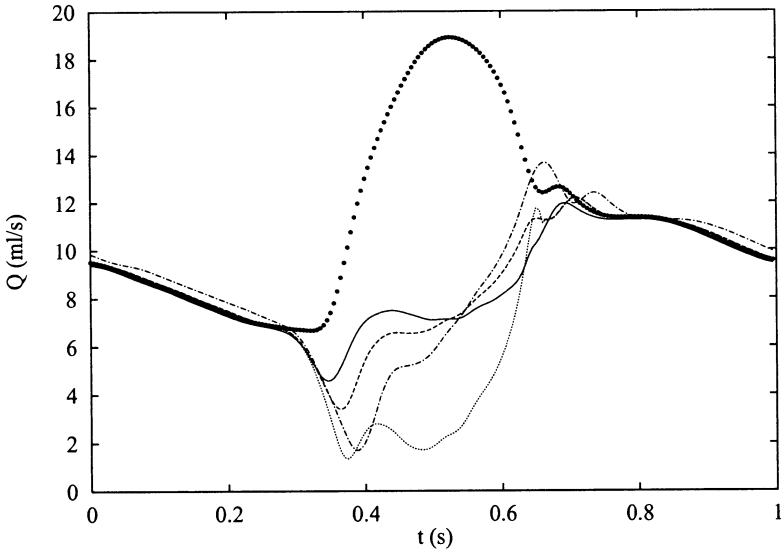

Figure 7: Total arterial flow into the root segment of the CCO tree of Fig. 1. Without myocardial squeezing (circles, showing increasing flow during systole), and under different squeezing conditions (solid line: full squeezing, no time lag, identical to the topmost curve of Fig. 6; dashed and dash-dotted lines: full squeezing, 20 ms and 50 ms delay of the onset of AoP with respect to IMP; dotted line: pressure timing as in Fig. 5, but with a 10 % increase of IMP over LVP).

Key words

constrained constructive optimization
computer modeling
coronary hemodynamics
arterial compliance
analog network

References

1. Schreiner, W. Computer generation of complex arterial tree models, *Journal of Biomedical Engineering*, 1993, **15**, 148–150.

2. Podesser, B., Neumann, F., Neumann, M., Schreiner, W., Wollenek, G. & Mallinger, R. Outer radius-wall thickness-ratio, a quantitative histology of the human coronary arteries, *Microvascular Research*, submitted.

3. Schreiner, W. & Buxbaum, P. Computer-optimization of vascular trees, *IEEE Transactions of Biomedical Engineering*, 1993, **40**, 482–491.

4. Rodbard, S. Vascular caliber, *Cardiology*, 1975, **60**, 4–49.

5. Schreiner, W., Neumann, F., Neumann, M., End, A., Rödler, S.M. & Aharinejad, S. The influence of optimization target selection on the structure of arterial tree models generated by constrained constructive optimization, *Journal of General Physiology*, 1995, **106**, 583–599.

6. Fung, Y.C. *Biomechanics: Mechanical Properties of Living Tissues*, Springer-Verlag, New York, 1981.

7. Douglas, J.E. & Greenfield, J.C.J. Epicardial coronary artery compliance in the dog, *Circulation Research*, 1970, **27**, 921–929.

8. Gow, B.S. & Hadfield, C.D. The elasticity of canine and human coronary arteries with reference to postmortem changes, *Circulation Research*, 1979, **45**, 588–594.

9. Neumann, M., Neumann, F., Podesser B., Karch R. & Schreiner W. Simulation of coronary hemodynamics in a spatially resolved computer model of the arterial tree, in preparation.

10. Rooz, E., Wiesner, T.F. & Nerem, R.M. Epicardial coronary blood flow including the presence of stenosis and aorto-coronary bypasses - I: Model and numerical method, *Journal of Biomechanical Engineering*, 1985, **107**, 361-367.

11. Wiesner, T.F., Levesque, M.J., Rooz, E. & Nerem, R.M. Epicardial coronary blood flow including the presence of stenosis and aorto-coronary bypasses - II: Experimental comparison and parametric investigations, *Journal of Biomechanical Engineering*, 1988, **110**, 144-149.

12. Milnor, W.R. *Hemodynamics*, 2nd edition, Williams & Wilkins, Baltimore, 1989.

13. Rideout, V.C. *Mathematical and Computer Modeling of Physiological Systems*, Prentice Hall, Englewood Cliffs NJ, 1991.

14. Cromer, A. Stable solutions using the Euler approximation, *American Journal of Physics*, 1981, **49**, 455-459.